Available online at www.sciencedirect.com
SCIENCE DIRECT®
Remote Sensing of Environment 89 (2004) 83–94
Remote Sensing of Environment
www.elsevier.com/locate/rse

Surface characterisation of the Dome Concordia area (Antarctica) as a potential satellite calibration site, using Spot 4/Vegetation instrument

Delphine Six[a], Michel Fily[a,*], Séverine Alvain[b], Patrice Henry[c], Jean-Pierre Benoist[a]

[a] *Laboratoire de Glaciologie et Géophysique de l'Environnemlent, CNRS/UJF, 54 rue Molière, BP 96, 38 402 Saint Martin d'Hères Cedex, France*
[b] *Laboratoire des Sciences du Climat et de l'Environnement, CEA/CNRS, L'Orme des Merisiers, CE Saclay, Bat. 709, 91 191 Gif-sur-Yvette, France*
[c] *Centre National d'Etudes Spatiales, Division Qualité et Traitement de l'Imagerie Spatiale, Capteurs Grands Champs, 18 Avenue Edouard Belin, 33 401 Toulouse Cedex 4, France*

Received 7 July 2003; received in revised form 10 October 2003; accepted 14 October 2003

Abstract

A good calibration of satellite sensors is necessary to derive reliable quantitative measurements of the surface parameters or to compare data obtained from different sensors. In this study, the snow surface of the high plateau of the East Antarctic ice sheet, particularly the Dome C area (75°S, 123°E), is used first to test the quality of this site as a ground calibration target and then to determine the inter-annual drift in the sensitivity of the VEGETATION sensor, onboard the SPOT4 satellite. Dome C area has many good calibration site characteristics: The site is very flat and extremely homogeneous (only snow), there is little wind and a very small snow accumulation rate and therefore a small temporal variability, the elevation is 3200 m and the atmosphere is very clear most of the time. Finally, due to its location, it is frequently within view of many satellites. VEGETATION visible blue channel data (0.43–0.47 μm) of a 716×716 km^2 area centred on the French–Italian Dome Concordia station, during the 1998–1999, 1999–2000, 2001–2001, and 2001–2002 austral summers were cloud masked and atmospherically corrected. The snow surface Bidirectional Reflectance Distribution Function is very high with little spatial and seasonal variability, which is a major advantage for sensor calibration. The inter-annual variation is found to be very small, proving that the stability of the site is very good.

Keywords: Surface characterisation; Dome Concordia area (Antarctica); Satellite calibration; Spot 4/Vegetation instrument

1. Introduction

A reliable interpretation of remote sensing data requires a good calibration of satellite sensors: Absolute calibration to quantify emitted and reflected energy from the surface, inter-calibration to compare responses obtained from different sensors or different channels of the same sensor, and time variations of these components to determine drifts in the measurements' quality. Many methods exist for these different purposes such as pre-flight measurements, onboard calibration lamps, sun glint and uniform ground targets (generally deserts) such as White Sands (USA) or Sahara (Cabot, Hagolle, & Henry, 2000; Cosnefroy, Leroy, & Briottet, 1996; Hagolle, Barnes, Cabot, Meygret, & Henry, 2001; Hagolle et al., 1999; Kaufman & Holben, 1993; Staylor, 1990; Teillet et al., 2001). Desert targets are often considered because they are spatially homogeneous and temporally stable due to their almost total lack of vegetation (Wu & Zhong, 1994). However, different sources of errors could sometimes limit their use, like blowing dust or other changes in atmospheric conditions (Rao & Chen, 1995, 1996).

In the past few years, several studies have investigated the use of the large Antarctic and Greenland ice sheets to determine temporal changes of satellite sensors. All of these previous works using snow or ice targets for calibration focused on visible and near-infrared bands, as the snow reflectance is high for these wavelengths, at the opposite to the low reflectances in the short-wave infrared. For example, Loeb (1997), Tahnk and Coakley (2001) and Masonis and Warren (2001) quantified the drift of the Advanced Very High Resolution Radiometer (AVHRR) sensors, carried onboard NOAA-9, 10, 11, and 14. Jaross (1993) also used ice sheets to test the calibration of the TOMS sensor (Total

* Corresponding author. Tel.: +33-4-76-82-42-35; fax: +33-4-76-82-42-01.
E-mail address: fily@lgge.obs.ujf-grenoble.fr (M. Fily).

0034-4257/$ - see front matter © 2003 Elsevier Inc. All rights reserved.
doi:10.1016/j.rse.2003.10.006

Ozone Mapping Spectrometer). The results of these studies suggested that the ice sheets can serve as ground calibration targets because the albedo variability of snow surfaces of the Antarctic and Greenland high plateaus is very low at visible wavelengths. Grenfell, Warren, and Mullen (1994) showed from measurements done at South Pole and Vostok stations that the snow surface in Antarctica has a high albedo, in the range of 0.96–0.99, from 300 to 700 nm wavelengths. At visible wavelengths, this albedo is invariant with grain size and remained constant over the season, as long as there is no melting (Wiscombe & Warren, 1980).

Our objective is to study the Dome Concordia (or Dome C) area (75°S, 123°E), located on the East Antarctic plateau, as a potential ground calibration site (Fig. 1). This area has many characteristics, which are of interest for calibration. The snow surface is spatially homogeneous because surface roughness is weak with sastrugi (meter-scale longitudinal roughness) up to only 10–20 cm (Petit, Jouzel, Pourchet, & Merlivat, 1982), with a very low slope (<0.2°; Rémy, Shaeffer, & Legresy, 1999) and temporally stable due to a small snow accumulation rate and low wind (3.4 m/s in 1998; Keller, Weidner, Stearns, Whittaker, & Holmes, 2002). Atmospheric conditions are very clear most of the time, due to high altitude (>3000 m above sea level) and long distance from the coast (>1000 km), which implies a very low aerosol and water vapor content. Moreover, due to its latitude (75°S), this area is frequently viewed by many satellites and, in this respect, is better than South Pole, which is often not accessible due to the orbit inclination of sun-synchronous satellites. Finally, meteorological data are available at Dome C, and a future French–Italian station will soon begin year-round operations.

In this paper, we focus on the data acquired over the Dome C area, by the French SPOT4/Vegetation sensor since 1998 in the blue channel (named B0, 0.43–0.47 μm). After cloud removal and atmospheric corrections, spatial and temporal variations of the snow BRDF (Bidirectional Reflectance Distribution Function) are determined to test the quality of the Dome C surface as a ground target for sensor calibration. Finally, the inter-annual variations of reflectances are analyzed and interpreted in term of sensor drift.

2. SPOT4/Vegetation data processing

2.1. Sensor and data characteristics

The sun-synchronous SPOT4 satellite was launched in March 1998 with, onboard, the wide field of view imaging

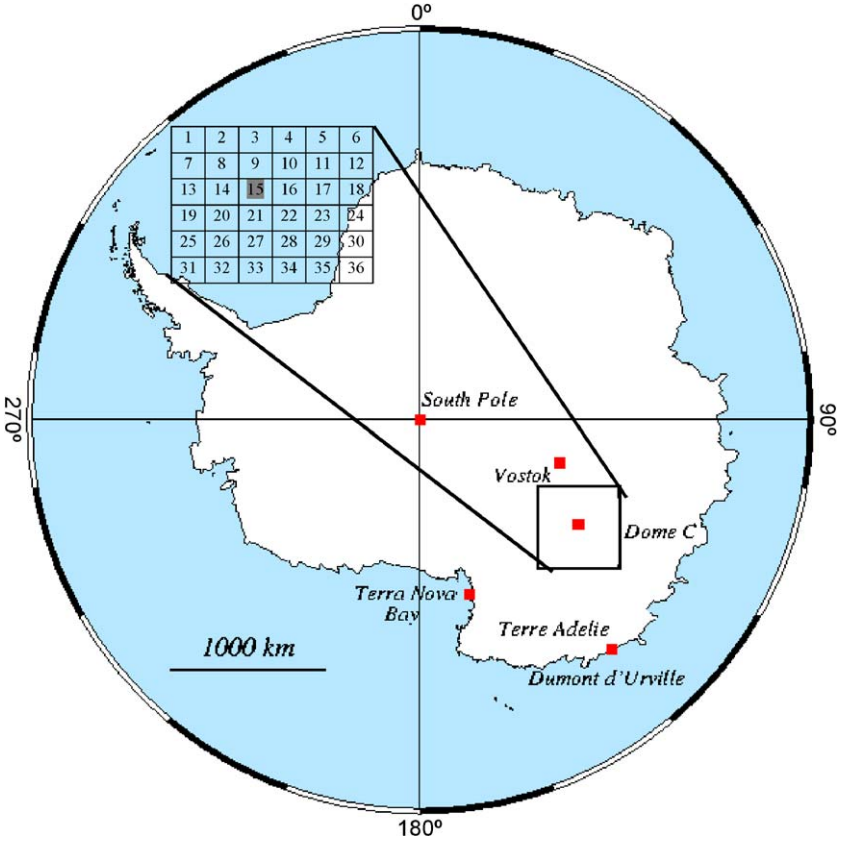

Fig. 1. Map of the Antarctic ice sheet, showing the selected 716 × 716 km^2 study area. The area is centered around the Dome Concordia international station (75°S, 123°E). On the left side of the picture are detailed the 36 grid boxes of 120 × 120 km^2 each, used for spatial variations studies. Dome C station is located in grid box number 15.

radiometer VEGETATION (VGT), which was specially designed to monitor land surface parameters. VGT is a linear-array push-broom system with 1728 detectors for each of the four channels providing a swath width of about 2250 km. The spectral bands of the four channels are given in Table 1. In-flight radiometric calibration of each of the four sensors is based on different methods: Onboard calibration lamp is selected as reference for monitoring changes in the cameras sensitivity over time. Calibration over Rayleigh scattering, sun glint, clouds or deserts are the complementary calibration methods. The estimated calibration accuracy is around 5% for absolute calibration, better than 2% for multi-temporal calibration and less than 3% for inter-band calibration (Henry & Meygret, 2001).

The ground resolution is 1.15 km independent of the viewing incidence angle. In ground processing, all pixels are re-sampled onto a regular grid (1 km × 1 km) in a polar stereographic projection. The VGT "level P" products that we used provide reflectance values at the top of the atmosphere after geometric and radiometric corrections. The top-of-atmosphere reflectance is defined as $(L_{sat}*\pi)/(E_0*\cos(\theta_s))$ where L_{sat} is the radiance measured at the satellite level, E_0 is the solar irradiance (corrected by the daily Earth–Sun distance) and θ_s, the solar zenith angle. The solar and viewing angles (zenith and azimuth in both cases) are given every 8 km. Details of the VGT sensor are summarized in Table 1 and more information can be found in Henry (1999) and on the Vegetation web site (http://vegetation.cnes.fr).

For this study, a 716×716 km^2 area centred on the Dome Concordia station is selected from the original swath (Fig. 1). At this latitude (75°S), data are available only for austral summer (November to February). The following images are available: 128 images during austral summer 1998–1999, 153 images for 1999–2000, 161 images for 2000–2001 and 569 images for 2001–2002. For the last season 2001–2002, six to eight images per day were programmed by CNES (*Centre National d'Etudes Spatiales*-Toulouse, France), instead of only one or two per day for the first three years. On the whole, 1011 images were available to statistically test Dome C and its surroundings as a ground calibration target.

Table 1
SPOT4/Vegetation sensor geometric and radiometric characteristics

Geometrical characteristics	
Orbital altitude	822 km
Period of resolution	101.46 min
Field of view	± 50°
Swath width	2250 km
Ground resolution	1.15 km
Pixel size	1 km
Spectral bands	
B0 (blue)	0.43–0.47 μm
B2 (red)	0.61–0.68 μm
B3 (near infra-red, NIR)	0.78–0.89 μm
B4 (short-wave infra-red, SWIR)	1.58–1.75 μm

There is no B1 channel onboard VGT in order to keep the same notation from SPOT1 to SPOT5.

2.2. Cloud masking

Even though clouds are rarely thick above the Antarctic plateau and their spectral signature is very similar to that of snow in the visible wavelengths, shadows or bright spots due to the rough texture of the top surface of clouds could affect the measured reflectance.

Our cloud detection algorithm uses two criteria developed in previous studies by Mondet and Fily (1999). The first criterion is based on the sensitivity of the reflectance to scattering particle size in the near-infrared channels (NIR and SWIR) (Fig. 1b of Masonis & Warren, 2001) and on the fact that snow grains are usually larger than cloud particles. High reflectances are associated with small particles and therefore with clouds. Rather than to apply a direct threshold on the reflectances in the SWIR channel which is the most sensitive to the grain size effect, we used the SWIR/NIR ratio, in order to minimize surface topography effects. In the ratio, the NIR channel is preferred instead of a visible one because it is less sensitive to atmospheric effects. The ratio threshold (SWIR/NIR = 0.25) was established from the visual analysis of a large number of images of the same area where snow surface patterns can be recognized when there is no cloud. This analysis shows that the same threshold is applicable for all 4 years.

The second criterion is based on the image texture, using the fact that the snow surface is often smoother than the cloud surface, so that the pixel-to-pixel variance over snow is lower than over clouds (Coakley & Bretherton, 1982). The variance is computed on a 25×25-pixel moving window in the B2 (red) channel in order to minimize the grain-size effects. The threshold is also chosen by visual analysis of many images, as was the first criterion.

A cloud is "detected" when at least one of these two criteria is true. Before atmospheric corrections, and because the solar and viewing angles are given only every 8 pixels, the 716×716-pixel images are reduced to 89×89-pixel images by averaging the reflectance values in each 8×8-pixel area. An 8×8-pixel cell is then considered to be cloudy if more than 32 initial pixels (50%) were classified as cloudy because we have considered that, in this condition, the number of data is too small to compute a mean reflectance. If less than 50% of the pixels are considered as cloudy, the mean reflectance is then computed only from the clear pixels. An example of cloud detection is given in Fig. 2, for a particular image acquired by VGT on December 24, 1999. The rough cloud texture appears in the bottom right part of the B0 image (left side of Fig. 2) and the high cloud reflectance in white color in the SWIR channel (middle of Fig. 2).

Fig. 2. Example of a SPOT4/VGT image acquired on December 24th 1999 over Dome C. The size of the image is 716 × 716 km^2 (Fig. 1). From left to right: B0 (blue) channel, SWIR channel, and final cloud mask using the SWIR/NIR ratio and the image texture. The clouds appear in black.

2.3. Atmospheric corrections

A method based on the inverse atmospheric radiative transfer model 6S (*Second Simulation of the Satellite Signal in the Solar Spectrum*; Vermote, Tanre, Deuze, Herman, & Morcrette, 1997) is then used to estimate ground reflectances from the Top Of Atmosphere (TOA) measurements of each VGT image. Instead of Masonis and Warren (2001) who got the reflectance of the sub-ozone layer, we preferred to estimate ground reflectances, as ground measurements of directional reflectance patterns will soon be conducted at Dome C station to assess the absolute calibration of the sensor.

Beforehand, it was necessary to find out the best atmospheric characteristics for the area. First, attention was focused on the sensitivity of reflectances to extreme variations of temperature and water vapor at this location. As no measured atmospheric profile is available in this region, data from the ECMWF (*European Centre for Medium Weather Forecasting*) operational analyses (Gibson et al., 1997) and a few surface pressure measurements from Dome C station were used. The reflectance variations are less than 1% between extreme realistic atmospheric conditions. Therefore a single temperature and water vapor profile is used with an integrated water vapor content of 0.07 g/cm^2 in agreement with more recent studies (Chamberlin, 2001).

The same conclusion was reached about the effect of the target altitude, which is another input to 6S. The study was based on a topographic map of the area from ERS-1 satellite produced by the French *Laboratoire d'Etudes en Géophysique et Océanographie Spatiale* (Rémy et al., 1999). Altitudes vary from 2900 to 3400 m for our study area, but these variations do not modify significantly the atmospheric corrections. The altitude is then set at 3200 m which corresponds to Dome C. The slopes, very gentle for the area under study, are not taken into account in 6S.

Other parameters in 6S are the atmospheric aerosol loading and the aerosol optical thickness (AOT). Four types of aerosols are considered in 6S: Dust, soluble particles, oceanic particles and soot. There are very few aerosol measurements in Antarctica and they are mainly located near the coasts (Bodhaine, Deluisi, Haris, Houmere, & Bauman, 1986; Hansen, Bodhaine, Dutton, & Schnell, 1988; Minikin et al., 1998; Wagenbach, Legrand, Fischer, Pichlmayer, & Wolff, 1998; Warren & Clarke, 1990; Wolff, Legrand, & Wagenbach, 1998). From available data, the balance between the four types of aerosols was defined as followed: 0% dust, 70% sulfates, 30% oceanic, 0% soot. Sensitivity analysis showed that a variation in this distribution has negligible effects (lower than 1%). There are very few measurements of optical thickness in Antarctica and data from the AERONET network (*Aerosol Robotic Network*; Holben et al., 1998, 2001) at Mc Murdo station were used for its determination. Without any additional ground information, a constant value of 0.06 (at 550 nm) was chosen for the optical thickness. This needs to be assessed in the future by ground measurements at Dome C.

A look-up table was created that provides ground reflectance to the corresponding TOA reflectance for all the geometric conditions (solar and viewing angles) that could be encountered over the 716 × 716 km^2 area. An example of atmospheric correction is given in Fig. 3, for a cloud free image in B0 channel acquired on December 28, 1999. We notice an increase of reflectance values after correction, up to 10%. Values are then close to in situ measurements made at Amundsen-Scott (South Pole) and Vostok stations on the Antarctic continent (Grenfell et al., 1994). There is less spread of the ground reflectance values after atmospheric corrections because the TOA reflectances depend on the path length through the atmosphere. Indeed, the three peaks observed before corrections are smoothed and barely seen after corrections.

2.4. BRDF data base

The snow surface reflectance values derived from VGT measurements in the B0 spectral band after cloud masking and atmospheric corrections are now used to prepare a ground reflectance data set which is the basis of the data analysis. The data base contains the mean snow reflectance, the standard deviation of this mean reflectance and the total number of reflectance values for a given geometric condi-

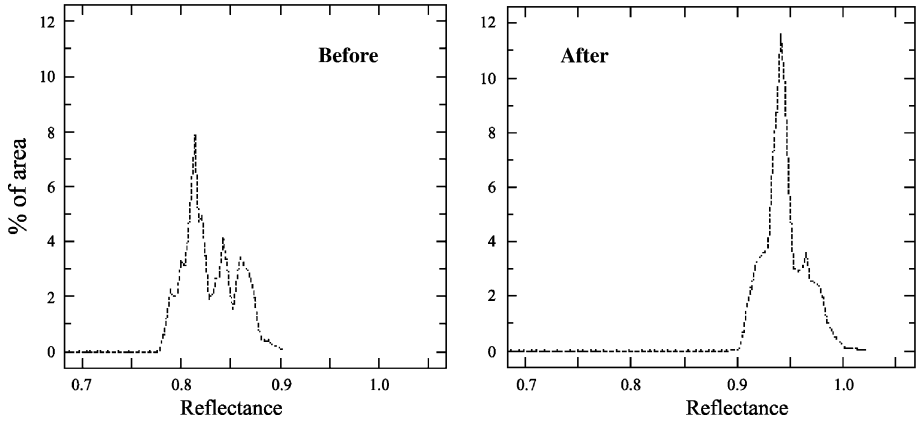

Fig. 3. Example of distribution of snow reflectances before (left) and after (right) atmospheric corrections on a clear-sky image acquired on December 28, 1999, in the blue channel.

tion (specified by four angles: Solar zenith angle θ_s, viewing zenith angle θ_v, solar azimuth angle Φ_s and viewing azimuth angle Φ_v), for a given month of each austral summer (4 months in each of 4 years), and for a given geographic grid-box. To balance the desire for spatial resolution against the need for good statistics, we chose to use a grid-box of 120×120 km^2, resulting in 36 grid-boxes in our primary 716×716 km^2 area (see Fig. 1). The size of the grid-box is close to that used by the CNES over deserts, typically 100×100 km^2. The four summer months (from November to February) are studied independently in order to take into account a possible evolution of the snow surface during the season.

Bins of small angular range are defined. For each bin, the average reflectance and its standard deviation are obtained. The chosen angle increments are: 2° for the solar zenith angle (θ_s), 5° for the viewing zenith angle (θ_v) and 20° for the azimuth angles (Φ_s and Φ_v). As θ_s varies between 82° and 50° during the summer at the time of data acquisition, generally in the morning, 17 bins of θ_s are represented in the data base. All measurements with θ_s>82° are discarded because the atmospheric effects are large and uncertain when the sun is so low. The local VGT viewing zenith angles (θ_v) range from nadir to 60° or from nadir to −60°, giving 26 different possibilities, depending on whether the sun and the satellite are in the same azimuth hemisphere.

This ground reflectance data base as a function of month, year, and grid-box, is now used to derive the main spatial and temporal radiometric characteristics of the area around Dome C, in the B0 spectral band.

3. Snow reflectance analysis over the Dome C area

As only a few orbits were selected for data acquisition over the Dome C area and because SPOT4 is a sun-

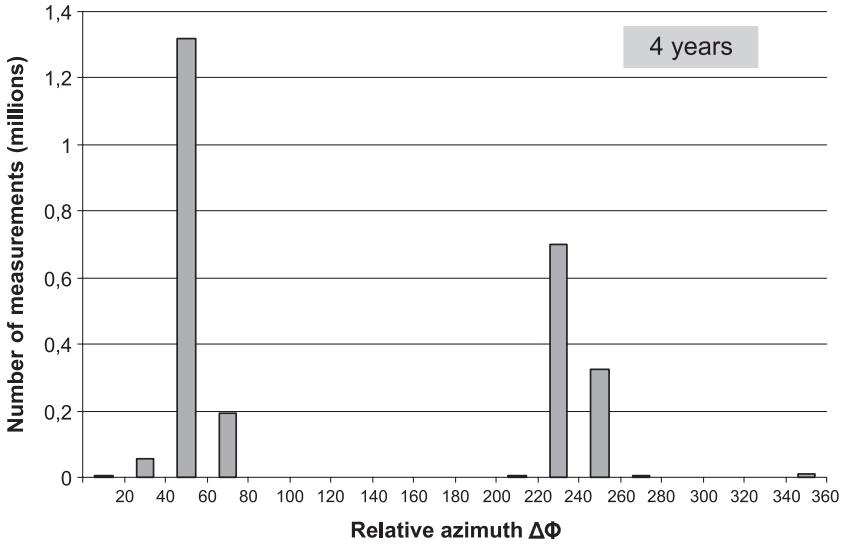

Fig. 4. Histogram of the relative azimuth angles between the sun and the satellite ($\Delta\Phi = \Phi_s - \Phi_v$). All the available data (after cloud masking, between 1998 and 2002 and over the selected study area) are used (1011 images).

synchronous satellite, not all solar and viewing azimuth angles are available in our data set. The histogram of the relative azimuth angles between the sun and the satellite ($\Delta\Phi = \Phi_s - \Phi_v$) for the 1011 images of the data base is given in Fig. 4. Most of the measurements were made in a relatively narrow range of angles: Between 50° and 90° in the backward scattering hemisphere (the sun and the satellite are in the same hemisphere, θ_v is then arbitrarily taken as negative) and between 230° and 270° in the forward scattering hemisphere (θ_v is then positively defined). As our ultimate objective is the VGT calibration, the following analysis is restricted to those azimuth angles where most of the data are found. In this narrow range, the reflectance is considered as almost independent of the azimuth in a given scattering hemisphere (backward or forward) as found from ADEOS/POLDER data (Mondet & Fily, 1999). The other data were not used, thus avoiding the variability which could be due to the azimuth angle. All the viewing angles θ_v were kept because VGT is a push-broom array system and all the detectors of the sensor must be calibrated.

3.1. Overall results

All the data (1011 images, 4 years × 4 months × 36 grid-boxes), for the selected $\Delta\Phi$, are first gathered to give an overall view of the snow reflectance in this region (Fig. 5a). Its variability, expressed as the standard deviation of the reflectance value in a given angular bin is presented in Fig. 5b. The number of data N for a particular bin is also given in the same (θ_s, θ_v) space (Fig. 5c).

The measured reflectance varies between 0.96 and 1.04 for our complete data set. These observations are in the range of the published data at South Pole station: Spectral albedos (directional-hemispheric reflectance) are given in Grenfell et al. (1994) and bi-directional reflectance functions patterns from ground measurements in Warren, Brandt, and O'Rawe Hinton (1998). The higher reflectances are found at large viewing angles in the forward and backward scattering directions in accordance with previous results and models. As snow grain size is larger than the wavelength of solar illumination (typically 50–100 μm for the snow grains in Antarctica, compared to 0.5 μm for solar radiation), the single-scattering asymmetry factor is very high and the consequence is that the phase function of a snow surface exhibits a strong forward peak (Warren et al., 1998; Wiscombe & Warren, 1980). This is generally strengthened as solar zenith angle increases but our study shows that the effect of the solar zenith angle is pretty small in the range of the available observations (50–82°). A minimum reflectance is found close to nadir views as expected. This minimum nadir reflectance, and the strongest forward-scattering peak are both found for a solar zenith angle $\theta_s = 72°$, which does not correspond to the maximum solar zenith angle because at large solar zenith angles the diffuse part of the irradiance is larger than the

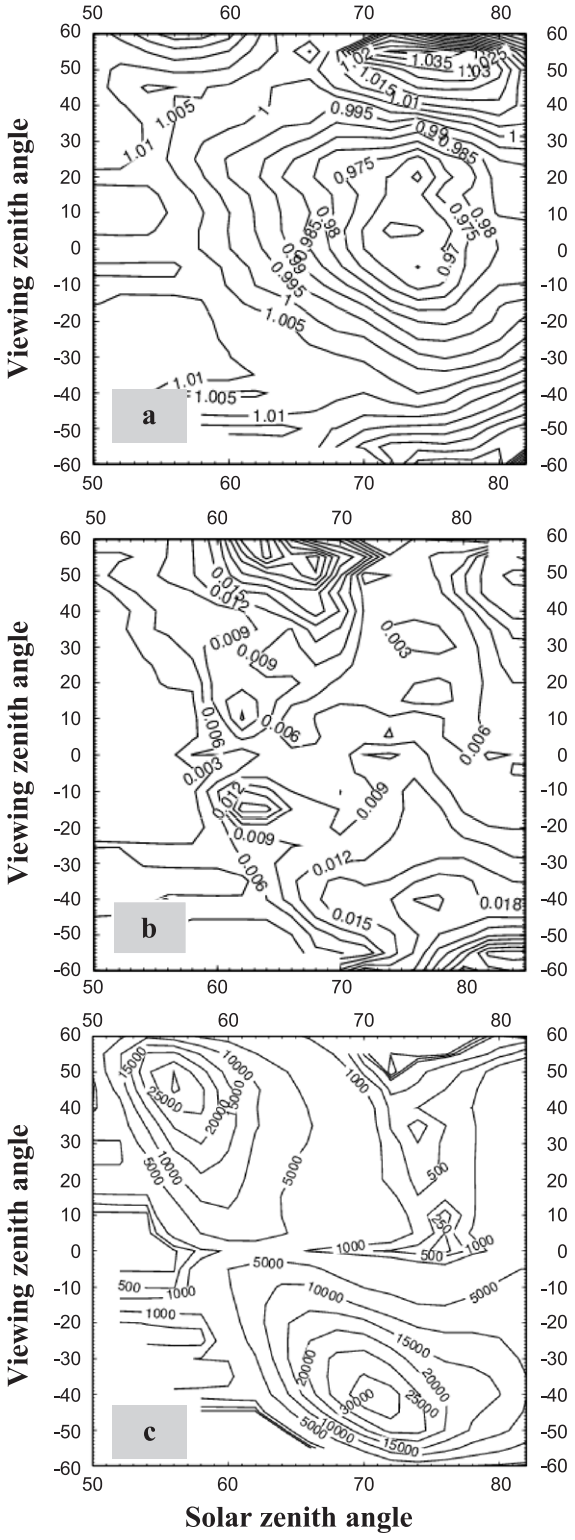

Fig. 5. Reflectance values (a), standard deviation of the reflectances (b) and number of measurements (c) as a function of solar zenith angle θ_s (on the horizontal axis) and viewing zenith angle θ_v (on the vertical axis), for the 1011 images. θ_v is defined to be positive when $\Delta\Phi$ is between 230° and 270° (forward scattering hemisphere) and negative when $\Delta\Phi$ is between 50° and 90° (backward scattering hemisphere).

direct one. This minimum also varies with month of observation, as described below.

The variability of the reflectance (Fig. 5b) is very small, less than 3% for almost angles and less than 1.5% for viewing angles within 30° of nadir. This small variability is very advantageous for sensor calibration. We can also observe that, as in other BRDF studies, the variability of the reflectance is somewhat smaller in the forward-hemisphere near-nadir views (Masonis & Warren, 2001; Warren et al., 1998). Higher values are found for large incidence angles, as found also by Masonis and Warren (2001), for many reasons: Topographic variations have a larger effect on the irradiance, surface roughness induces more local variations (shadows and bright spots), atmospheric effects are more important on both the sun-surface and the surface-satellite paths. Another reason is that the data sampling is based on fixed ranges of angles when the irradiance and the radiance are instead related to the cosine of the zenith angles: The same angle variation of 5° corresponds to a cosine variation of 0.01 between 5° and 10° and of 0.08 between 65° and 70°.

Fig. 5c shows that the measurements are not uniformly distributed in (θ_s, θ_v) space, but that there are still many measurements at large θ_s and large θ_v. We computed a reflectance for a bin only if at least 10 measurements were made.

3.2. Seasonal variations

The snow surface on the plateau can evolve slightly during the summer due to solar radiation and sublimation (Gow, 1965) more than due to changes in atmospheric conditions. In fact, the temperature is always below freezing over the Antarctic plateau (Warren, 1996). Dome C 2002–2003 records show that the temperature varied between −30 °C in December 2002 and −35 °C in January 2003 and the wind is weak (averaging 3.4 m/s in 1998, Keller et al., 2002). No a priori large modification of the surface is

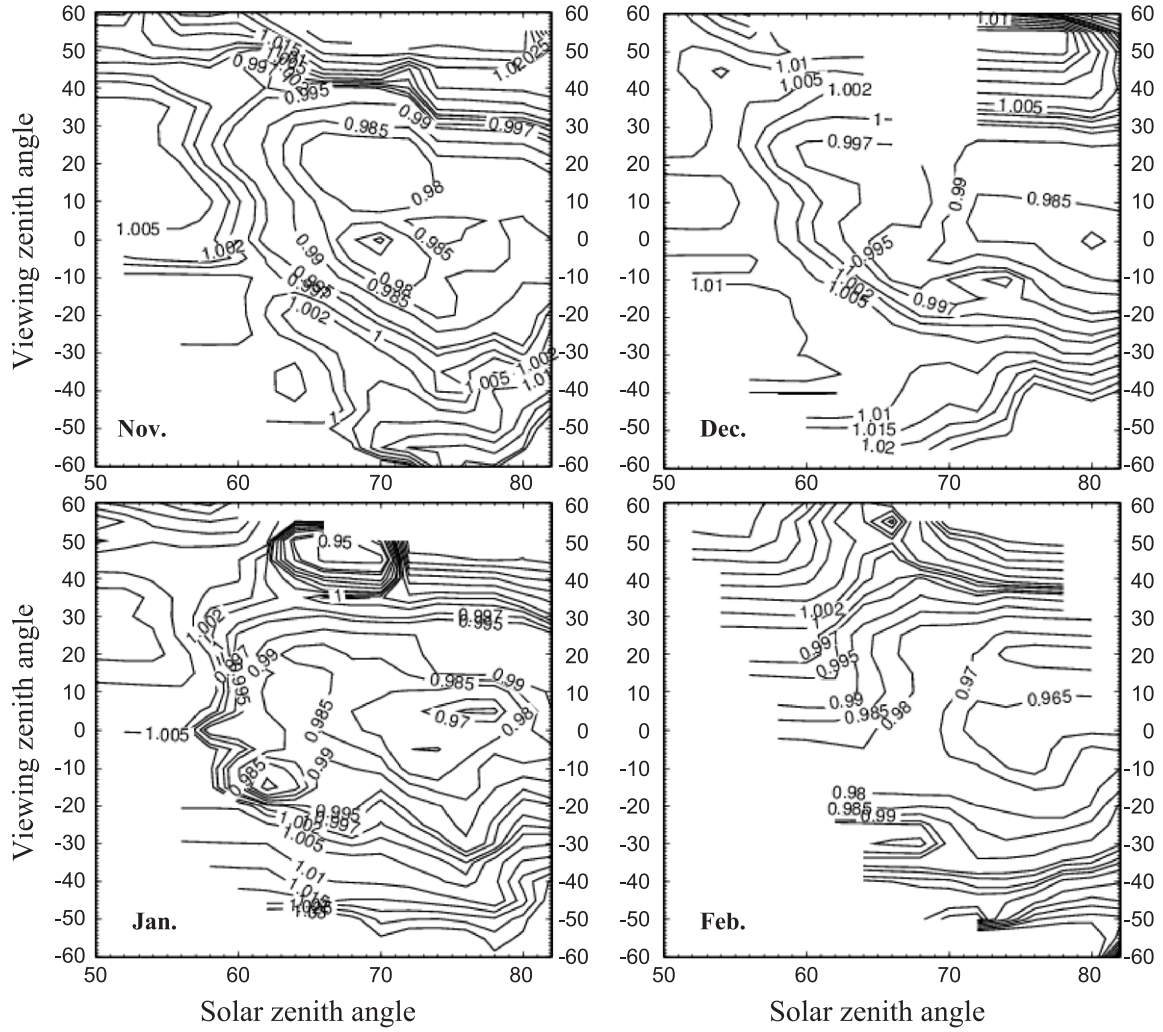

Fig. 6. Reflectance values for November, December, January and February, as a function of solar zenith angle θ_s (on the horizontal axis) and viewing zenith angle θ_v (in the backward and forward hemispheres).

then expected but, as no specific ground observations are yet available around Dome C, and also because the distribution of solar zenith angles changes during the summer, a seasonal study of the VGT data is conducted by comparing results from the four summer months (November, December, January and February). For each month, all the corresponding data are gathered: 4 years × 36 grid-boxes. The mean ground reflectances for each month are given in Fig. 6 in the same (θ_s, θ_v) space as in Fig. 5. As expected the reflectance differences between the 4 months for a particular geometric condition are very small, less than 0.02 in most cases. Exceptional low values are found when the solar zenith angle is around 68° in the forward scattering direction, this is due to only a few measurements. As said before, a minimum of reflectance appears at nadir for large solar zenith angles but not always for the same angle. Slightly lower reflectances are found in February but the reason is still unknown. It seems that the snow grain size does not really change over the season as the forward peak is not more pronounced at the end of the season compared to the beginning.

In contrast, there are more differences between the monthly variabilities. In Fig. 7 is given the mean variability (standard deviation) of the measured reflectances for solar zenith angles in the range 60–66°. As said before, a minimum variability is found close to nadir. In November and in December the variability is always small, less than 0.02, in all years. Relatively large standard deviations are found in January and February for 1999–2000 and 2001–2002. The yearly differences in variances observed for January and February compared to November and December were statistically tested and are significant at a 95% level. This lower variability for December was also noticed by Masonis and Warren (2001) but this is not explained so far. One reason could be that solar zenith angles are generally lower in December than in February or early November. The second one could be that there are more clouds in January or February and even if they are removed, some of them could

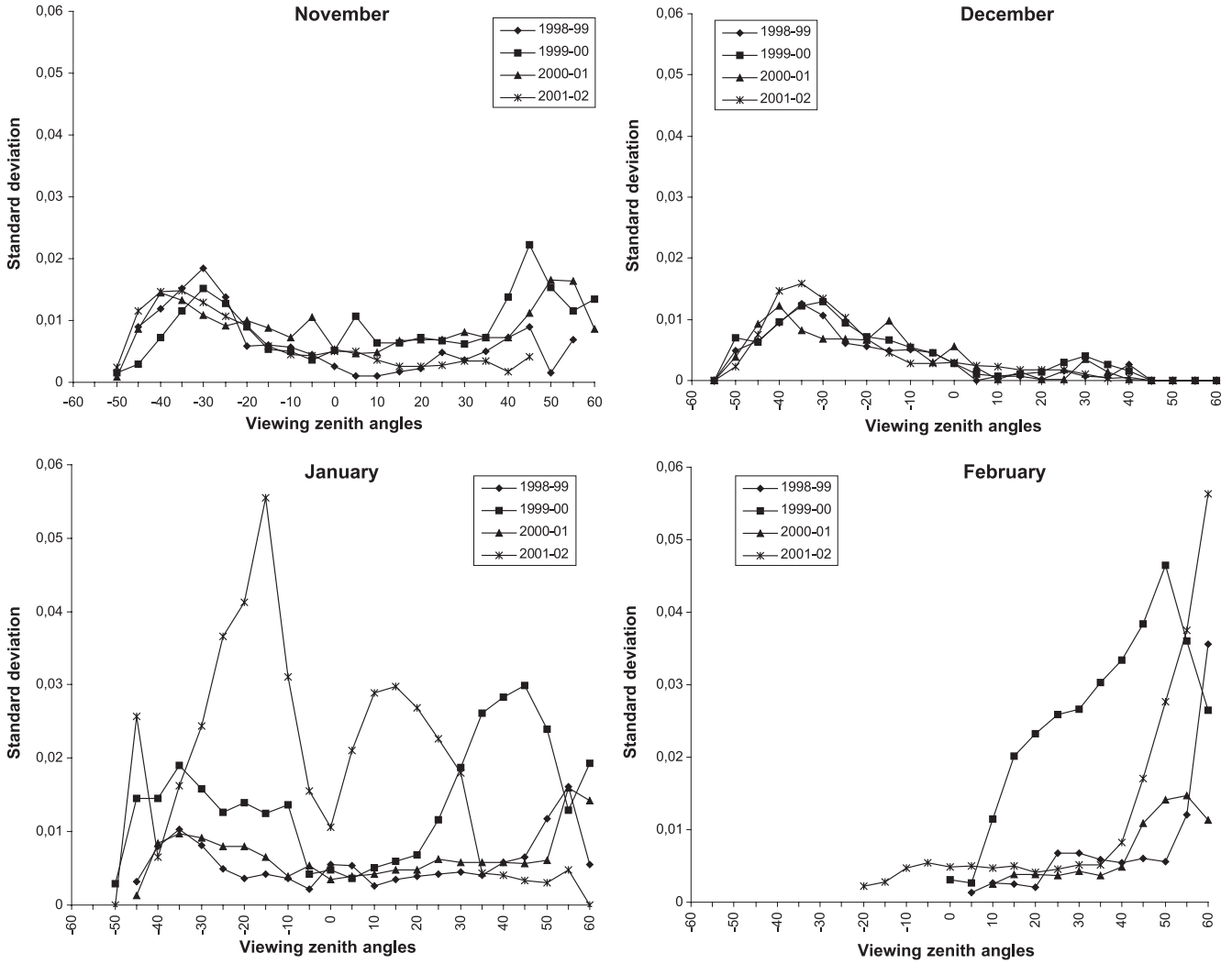

Fig. 7. Standard deviation of snow reflectances as a function of viewing zenith angle θ_v, for each month (November, December, January and February) of every year. Data are gathered over the total 716 × 716 km^2 area (36 zones). Solar zenith angles θ_s vary between 60° and 66° in this particular example.

Table 2
Percentage of cloudy pixels for each month of each year (1011 images)

	November	December	January	February
1998–1999	52%	50%	70%	70%
1999–2000	51%	50%	42%	58%
2000–2001	33%	59%	59%	57%
2001–2002	49%	60%	84%	74%
Average	46%	55%	64%	65%

still exist in the reflectance data base. The cloud coverage was therefore analyzed from the 1011 images (Table 2).

We observe that, on average, there are more clouds in January and February than in November and December but that 1999–2000 was less cloudy. Therefore, the cloud coverage is probably not the only reason for this larger variability. Another explanation could be a modification of the snow surface, different from the normal seasonal evolution of the sastrugi described by Gow (1965). Formation of surface hoar through the summer has been observed in some places on the plateau. More in situ observations are needed before anything more definite can be said.

In any case, for sensor calibration, the December and November data will be preferred because they show a remarkable stability with a standard deviation always less than 0.02. Another advantage of December is to provide the smallest solar zenith angles, thus minimizing topographic and atmospheric effects.

3.3. Spatial variations

From different VGT images in the solar spectrum or from the new RAMP (*Radarsat Antarctic Mapping Mission*) mosaic of SAR (*Synthetic Aperture Radar*) images in the microwave domain (http://nsidc.org/data/nsidc-0103.html),

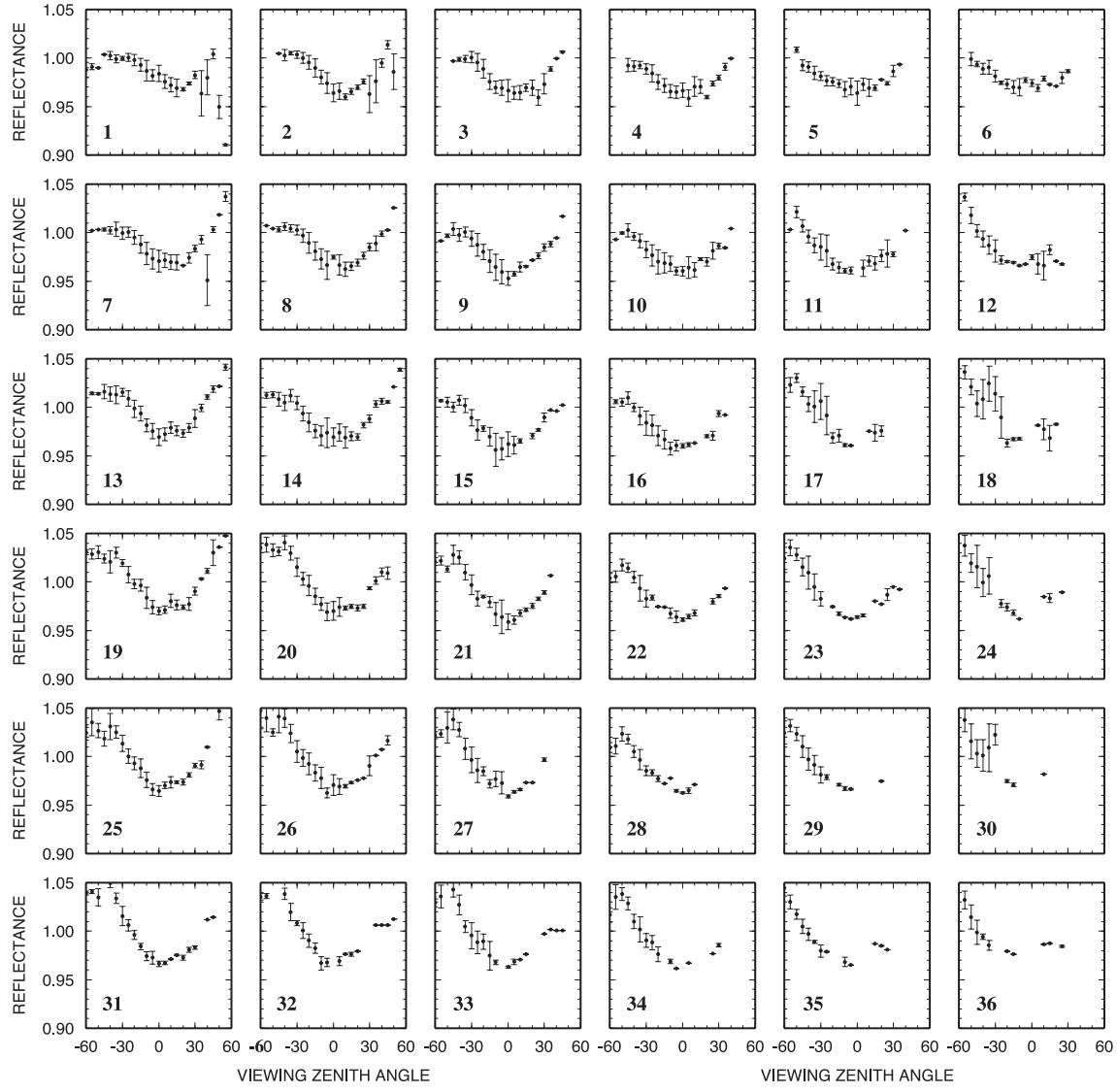

Fig. 8. Measured mean snow reflectances in each of the 36 zones as a function of viewing zenith angle θ_v (zones 1–36, from South to North as shown on Fig. 1). Data are gathered for 4 months × 4 years. Errors bars represent ± 1 × standard deviation. In this example, solar zenith angles θ_s are between 68° and 74°.

it can be seen that the surface is not perfectly homogeneous over the entire 716×716 km^2 area. Large surface dunes occur in some parts of our domain, on 100-km scale. Therefore, it is necessary to look at the spatial variation of the snow reflectance and of its variability in order to determine whether some places are more suitable for sensor calibration. In Fig. 8 are given the measured mean snow reflectances, all the 16 months combined, in the 36 grid-boxes as they appear in Fig. 1: The top left graph corresponds to the South zone 1 and the bottom right to the North zone 36. The reflectance is given versus the viewing angle ($\theta_v < 0$ for backward hemisphere and >0 for forward hemisphere) for one range of sun incidence angles: $68° < \theta_s < 74°$. Similar results are obtained if different solar zenith angle ranges are selected. The error bars correspond to $\pm 1 \times$ standard deviation.

The top-left zones (South) correspond to the less rough area. A more pronounced forward scattering peak is found there corresponding to a smooth snow surface. A rougher surface is found for the bottom-left zones (North–East) with a generally more pronounced backward scattering peak as in Mondet and Fily (1999). But although the BRDF varies spatially, reflectance variability does not, i.e. the error bars do not differ significantly from one grid-box to another. From these 4 years of acquisition, we therefore have no reason to select a particular box or set of boxes for calibration purpose, even if areas of the top half of the pictures are more flat, without roughness, and are therefore probably less sensitive to inter-annual variations. However, as field campaigns are also planned in the future at Dome C to determine surface and atmospheric characteristics, and as the CNES does not need such a large area as the initial 716×716 km^2, it is then

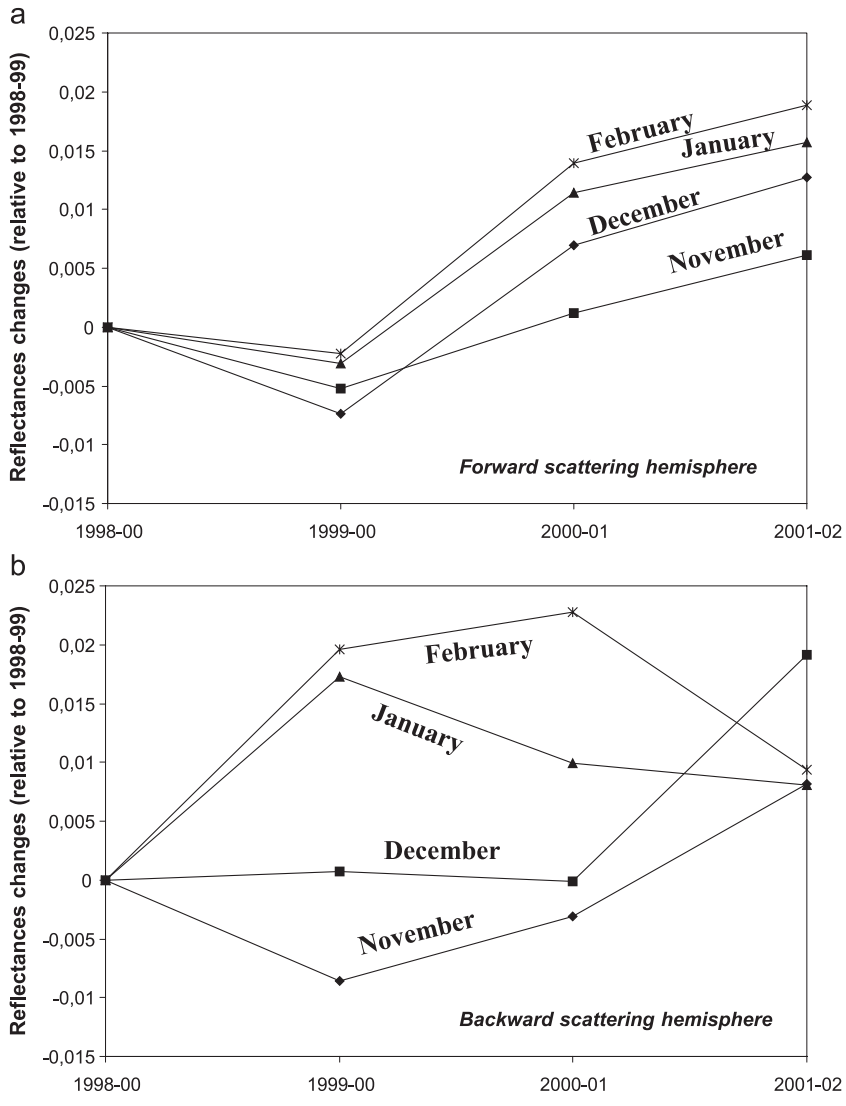

Fig. 9. Annual variability of the median of the inter-annual differences of reflectance values for each month with year 1 (1998–1999) as a reference. Differences are computed between reflectances measured with same geometric conditions. The top of the figure (a) represents the median of the differences in the forward hemisphere (range of θ_v is [30°, 60°]), and the bottom (b), in the backward hemisphere (range of θ_v is [−30°, −60°]).

reasonable to propose the sensor calibration work on a restricted area around Dome C.

3.4. Inter-annual variations

As mentioned by Masonis and Warren (2001), the snow surface of the high Antarctic plateau should not change significantly from 1 year to the other. Based on this assumption, inter-annual analysis should allow assessment of the sensor's drift over time. Previous sections show that there are differences between the 4 months if the variability is considered and differences between the 36 boxes if the reflectance is considered. Moreover, distribution of solar and viewing angles is different with space and time. Therefore, for inter-annual variations, similar data must be compared: Same sun-satellite geometry, same box and same month. For data of the same region, for each combination of θ_s, θ_v and $\Delta\phi$, only when data are available in all 4 years, the change of monthly mean reflectance is computed from the first summer (1998–1999) to each of the three subsequent summers, for data of the same region. In order to avoid spurious data, the reflectances smaller than 0.85 are rejected as well as the data with a standard deviation greater than 0.03, which seems reasonable for snow surface in this region, considering the average value of the standard deviation. From the distribution of differences, the mean and the median of inter-annual differences are then computed.

The median of the inter-annual differences is given for each month in the backward hemisphere (Fig. 9a) and in the forward hemisphere (Fig. 9b). Very similar results are found with the mean differences. The first comment is that the inter-annual variability is very small, less than 2% over 4 years. As noted earlier, variability is lower in the forward hemisphere. As the available reflectances were already calibrated with the onboard calibration lamp and over classic desert targets, our study then shows that a high confidence level can be given to the actual Vegetation calibration.

4. Conclusion

An analysis of 1011 images acquired by SPOT4/Vegetation sensor was made to assess the variability of the snow surface reflectance of the high Antarctic plateau over four consecutive austral summers, from 1998–1999 to 2001–2002. Each image covers an area of 716×716 km^2, centered on the French–Italian Dome Concordia station (75°S, 123°E). This data set allows statistical inter-annual analysis to test the quality of this area as a calibration site and to determine the drift of the VGT sensor over the 4 years in the B0 (blue) channel.

First, we have demonstrated the utility of removing clouds from the pictures as the variability is then approximately divided by 2. Even if clouds are most of the time sparse or thin over the high plateau, bright spots and shadows could modify top of atmosphere reflectances and particularly near the edges of the clouds.

The main conclusion of this study is to show a high stability of the ground reflectances that is the most important characteristic for a calibration site: Most of the time the variability is less than 2%. Ground structures which could evolve seasonally appear to be present in some parts of the 716×716 km^2 study area. For calibration purposes, we then propose to restrict the site to the southern part of the selected area, in the vicinity of Dome C station where ground measurements will be available, even if there are no significant differences reflectance variability for the different parts of the area. We also noticed that November and December are generally more stable than January and February, possibly due to greater cloud cover in late summer, or to the formation of surface hoar on the ground. Inter annual reflectance variations are very small, only 2% on 4 years, showing that the actual VGT calibration using onboard lamp and desert targets is very good.

In the future, other VGT channels will be processed, taking into account the ozone amount for the B2 channel and the grain size variations for the B3 channel. Ground measurements will be done to assess the atmospheric and surface characteristics at Dome C station. The atmospheric characteristics will be determined by measuring ozone absorption and aerosol optical thickness over an entire season. These measurements will be useful for radiative transfer models used to infer ground reflectance from the reflectance measured at the top of the atmosphere. The snow surface BRDF will also be measured 24 h per day over the season from the top of a 33-m tower, to determine its daily variations and then giving a tool for absolute calibration of this sensor and other visible sensors in this region. The first ground season took place in 2002–2003, the main measurements will be acquired in 2003–2004.

Acknowledgements

This study was funded by the Centre National d'Etudes Spatiales (CNES, Toulouse-France), the French Programme National de Télédétection Spatiale and the French Polar Institute (IPEV). Steve Warren, through his useful comments, helped us to greatly improve this paper.

We thank the anonymous referees for their judicious and helpful remarks.

References

Bodhaine, B. A., Deluisi, J. J., Harris, J. M., Houmere, P., & Bauman, S. (1986). Aerosol measurements at the South Pole. *Tellus*, *38B*, 223–235.

Cabot, F., Hagolle, O., & Henry, P. (2000). Relative and multi-temporal calibration of AVHRR, SeaWiFS, and vegetation using POLDER characterization of desert sites. *International Geoscience and Remote Sensing Symposium*, *5*, 2188–2190.

Chamberlin, R. A. (2001). South Pole submillimeter sky opacity and correlations with radiosonde observations. *Journal of Geophysical Research*, *106*(D17), 20101–20113.

Coakley, J. A., & Bretherton, F. P. (1982). Cloud cover from high-resolution scanner data: Detecting and allowing for partially filled fields of view. *Journal of Geophysical Research*, *87*, 4917–4932.

Cosnefroy, H., Leroy, M., & Briottet, X. (1996). Selection and characterization of Saharan and Arabian desert sites for the calibration of optical satellite sensors. *Remote Sensing of Environment*, *58*, 101–114.

Gibson, J., Kallberg, K. P., Uppala, S., Noumara, A., Hernandez, A., & Serrano, E. (1997). ERA description. *ECMWF Re-Analysis Project Report Series, vol 1*. Reading, UK: ECMWF, 77 pp.

Gow, A. J. (1965). On the accumulation and seasonal stratification of snow at the South Pole. *Journal of Glaciology*, *5*, 467–477.

Grenfell, T. C., Warren, S. G., & Mullen, P. C. (1994). Reflection of solar radiation by the Antarctic snow surface at ultraviolet, visible and near-infrared wavelengths. *Journal of Geophysical Research*, *99*, 18669–18684.

Hagolle, O., Barnes, R. A., Cabot, F., Meygret, A., & Henry, P. (2001). Absolute calibration of spaceborne optical instruments using natural targets. In: M. Leroy (Ed.), *8th International Symposium: Physical Measurements and Signatures in Remote Sensing. ISPRS, Aussois* (pp. 135–144).

Hagolle, O., Goloub, P., Deschamps, P. Y., Cosnefroy, H., Briottet, X., Bailleul, T., Nicolas, J. M., Parol, F., Lafrance, B., & Herman, M. (1999). Results of POLDER In-Flight Calibration. *IEEE Transactions on Geoscience and Remote Sensing*, *37*, 3.

Hansen, A. D. A., Bodhaine, B. A., Dutton, E. G., & Schnell, R. C. (1988). Aerosol Black carbon measurements at the South Pole: Initial results. *Geophysical Research Letters*, *15*(11), 1193–1196.

Henry, P. (1999). The VEGETATION system: A global monitoring system on-board SPOT4. In: *Proceedings of the Euro-Asia Space Week on Cooperation in Space, ESA SP-430* (pp. 233–239).

Henry, P., & Meygret, A. (2001). Calibration of HRVIR and VEGETATION cameras on SPOT4. COSPAR 2000. *Advances in Space Research*, *28*(1), 49–58.

Holben, B. N., Eck, T. F., Slutsker, I., Tanré, D., Buis, J. P., Setzer, A., Vermote, E., Reagan, J. A., Kaufman, Y. J., Nakajima, T., Lavenu, F., & Jankowiak, I. (1998). AERONET—A federated instrument network and data archive for aerosol characterization. *Remote Sensing of Environment*, *66*, 1–16.

Holben, B. N., Tanré, D., Smirnov, A., Eck, T. F., Slutsker, I., Abuhassan, N., Newcomb, W. W., Schefer, J. S., Chatenet, B., Lavenu, F., Kaufman, Y. J., Vande Castle, J., Setzer, A., Markham, B., Clark, D., Frouin, R., Halthore, R., Karneli, N. A., O'Neill, N., Pietras, C., Pinker, R., Voss, G., & Zibordi, G. (2001). An emerging ground-based aerosol climatology: Aerosol optical depth from AERONET. *Journal of Geophysical Research*, *106*, 12067–12097.

Jaross, G. (1993). Ice radiance method for BUV instrument monitoring. In: *Proceedings SPIE, 2047, Atmospheric Ozone* (pp. 94–101).

Kaufman, Y. J., & Holben, B. N. (1993). Calibration of the AVHRR visible and near-IR bands by atmospheric scattering, ocean glint and desert reflection. *International Journal of Remote Sensing*, *14*, 21–52.

Keller, L. M., Weidner, G. A., Stearns, C. R., Whittaker, M. T., & Holmes, R. E. (2002). *Antarctic Automatic Weather Station data for the calendar year 1998*. Madison, WI: Space Science and Engineering Center, University of Wisconsin, 47 pp.

Loeb, N. G. (1997). In-flight calibration of NOAA AVHRR visible and near-IR bands over Greenland and Antarctica. *International Journal of Remote Sensing*, *18*, 447–490.

Masonis, S. J., & Warren, S. G. (2001). Gain of the AVHRR visible channel as tracked using bidirectional reflectance of Antarctic and Greenland snow. *International Journal of Remote Sensing*, *22*, 1495–1520.

Minikin, A., Legrand, M., Hall, J., Wagenbach, D., Kleefeld, C., Wolff, E. W., Pasteur, E. C., & Ducroz, F. (1998). Sulfur containing in coastal Antarctic aerosol and precipitation. *Journal of Geophysical Research*, *103*(D9), 10975–10990.

Mondet, J., & Fily, M. (1999). The reflectance of rough snow surfaces in Antarctica from POLDER/ADEOS remote sensing data. *Geophysical Research Letters*, *26*(23), 3477–3480.

Petit, J. R., Jouzel, J., Pourchet, M., & Merlivat, L. (1982). A detailed study of snow accumulation and stable isotope content in Dome C (Antarctica). *Journal of Geophysical Research*, *87*(C6), 4301–4308.

Rao, C. R. N., & Chen, J. (1995). Inter-satellite calibration linkages for the visible and near-infrared channels of the Advanced Very High Resolution Radiometer on the NOAA-7, 9 and 11 spacecraft. *International Journal of Remote Sensing*, *16*, 1931–1942.

Rao, C. R. N., & Chen, J. (1996). Post-launch calibration of the visible and near-infrared channels of the Advanced Very High Resolution Radiometer on the NOAA-14 spacecraft. *International Journal of Remote Sensing*, *17*, 2743–2747.

Rémy, F., Shaeffer, P., & Legresy, B. (1999). Ice flow physical processes derived from ERS-1 high-resolution map of Antarctica and Greenland ice sheet. *Geophysical Journal International*, *139*, 645–656.

Staylor, W. F. (1990). Degradation rates of the AVHRR visible channel for the NOAA-6, -7 and -9 spacecraft. *Journal of Atmospheric and Oceanic Technology*, *7*, 411–423.

Tahnk, W. R., & Coakley Jr., J. A. (2001). Improved calibration coefficients for NOAA-14 AVHRR visible and near-IR channels. *International Journal of Remote Sensing*, *22*(7), 1269–1283.

Teillet, P. M., Fedosejevs, G., Gauthier, R. P., O'Neill, N. T., Thome, K. J., Biggar, S. F., Ripley, H., & Meygret, A. (2001). A generalized approac to the vicarious calibration of multiple Earth observation sensors using hyperspectral data. *Remote Sensing of Environment*, *77*, 304–327.

Vermote, E. F., Tanre, D., Deuze, J. L., Herman, M., & Morcrette, J. J. (1997). Second simulation of the satellite signal in the solar spectrum: An overview. *IEEE Transactions on Geoscience and Remote Sensing*, *35*, 675–686.

Wagenbach, D., Legrand, M., Fischer, H., Pichlmayer, F., & Wolff, E. W. (1998). Atmospheric near-surface nitrate at coastal Antarctic sites. *Journal of Geophysical Research*, *103*(D9), 11007–11020.

Warren, S. G. (1996). *Antarctica, encyclopedia of climate and weather* (pp. 32–39). New York: Oxford Univ. Press.

Warren, S. G., & Clarke, A. (1990). Soot in the atmosphere and snow surface of Antarctica. *Journal of Geophysical Research*, *95*(D2), 1811–1816.

Warren, S. G., Brandt, R. E., & O'Rawe Hinton, P. (1998). Effect of surface roughness on bidirectional reflectance of Antarctic snow. *Journal of Geophysical Research*, *103*(E11), 25789–25807.

Wiscombe, W. J., & Warren, S. G. (1980). A model for the spectral albedo of snow: I. Pure snow. *Journal of Atmospheric Sciences*, *37*, 2712–2733.

Wolff, E. W., Legrand, M., & Wagenbach, D. (1998). Coastal Antarctic aerosol and snowfall chemistry. *Journal of Geophysical Research*, *103*(D9), 10927–10934.

Wu, A., & Zhong, Q. (1994). A method for determining the sensor degradation rates of the NOAA AVHRR channels 1 and 2. *Journal of Applied Meteorology*, *33*, 118–122.